BULLETIN OF APPLIED MECHANICS 4(16), 129-137 (2008)

Innovative concept of increasing dynamic stiffness of compliant structures by mechatronic approach

Martin Nečas, Michael Valášek †

***Abstract*— This paper deals with an innovative mechatronic concept as means to significantly increase dynamic stiffness of mechanical structures. This increase results as a consequence of active force piezoactuation within the system. The system is controlled by a state space and sliding mode controller (SMC) and demonstrates a significant increase in dynamic stiffness of the target part of the structure. Presented concept aims at machine tools sector where mechanical compliance poses a major obstacle in achieving higher transfer and cutting speeds. Experimental test rig was built in order to verify the proposed concept.**

***Index Terms* — compliant structures, dynamic stiffness, mechatronics, piezoactuation.**

I. INTRODUCTION

The research field of active vibration control tries to provide mechatronic technologies to decrease susceptibility of mechanical structures towards vibrations and hence increase their dynamic stiffness. It should be stated that the later is very important, since what we essentially want to achieve is a stiff lightweight structure (stiff in a wide range of excitation frequencies). The limiting factor here is typically the first eigenfrequency and therefore methods for its shifting or complete attenuation are of a great importance.

Active vibration control is a development that can be dated back to the introduction of microprocessor technology in the early 70ies with a development of sensor and actuator technology. These technologies enabled to close up the required mechatronic control loop and realize the required mechatronic function.

Major developments in the active vibration technology are motivated by production, aerospace, transportation and partially also by a construction industry. It should be noted that a passive (energy dissipating) vibration control solutions such as anti-vibration pads, coatings and automobile air and oil dampers are still prevalent mainly due to their simplicity and robustness.

† Manuscript received December 27, 2008. This work was supported in part by the GA ČR under Grant 101/08/P633, authors highly acknowledge the provided financial support.

M. Nečas is with the Czech Technical University in Prague, Karlovo nám. 13, Praha 2, 121 35, Czech Republic, phone: +420-224357513; fax: 224916709; e-mail: martin.necas@fs.cvut.cz.

M. Valášek, is with the Czech Technical University in Prague, Karlovo nám. 13, Praha 2, 121 35, Czech Republic,
e-mail: michael.valasek@fs.cvut.cz.

The research of active vibration control in areas of machine tools has mainly been driven through advancement in solid state actuators technology and associated power electronics, namely switched power amplifiers. The placement of discrete solid state actuators to control vibration of typically lightly damped structures (e.g. welded machine tool frames) along with linear motor technology presents the current state of the art [1] and is the first step to a development of composite materials with distributed sensing and force actuation capabilities. In the near future magnetic and solid state technologies are likely be the determining factors for the further improvement of machining productivity and precision.

The most predominantly used solid state actuation technology in active vibration control today is based on a Lead(Pb)-Zincornium(Zr)-Titanate(Toi) oxide ceramic (PZT) piesostacks. The maximum strain achievable today is about (1-2 ‰) and up to recently, large force (50000 N), limited stroke actuators were available (typically 30-150 μm). The most recently developed actuators achieve strokes of 1000 μm with forces ranging up to 70000 N and with a corresponding actuator length of 500 mm. Shortly achievable power output of such actuators can be up to 0.1 MW in 50 μs pulse [2] . The piezoelectric technology opens up the whole range of important applications. A very good example related to piezo active chatter reduction in deep hole drilling can be found in a work of Erdal Enver [3].

The structures of machine tools suffer from the conflict between required stiffness and dynamics. The consequence is limited accuracy and/or limited productivity of the manufacturing. The sufficient stiffness requires large amount of material to be used that in turn results in the increase of machine tool mass. The increased mass leads to the decrease of dynamics and machine tool productivity. On the other hand increase of dynamics typically requires a use of low mass structures. However, these structures have typically low stiffness and their first eigenfrequency is likely to lead to chatter problems and decreased accuracy. Traditional techniques to create lightweight high stiffness structures make typically use of structural optimization of advanced composite materials [4]. Synergically, this problem can also be solve through application of mechatronic solutions as illustrated in this article.

The paper is further organized further into five sections. The section 2 illustrates the concept of mechatronic stiffness followed by section 3 on system modeling and its control. The section 4 contains experimental verification and system identification followed by the section 5 with simulation results. The section 6 presents experimental results and the

overall results and outviews are summarized in the conclusion section.

II. INNOVATIVE CONCEPT OF MECHATRONIC STIFFNESS

Mechanical structures are compliant. Their stiffness can be increased by feedback control of a force from an actuator embedded within the structure. Based on the Newton law of action and reaction the actuator requires a support on the frame for exerting a force. The possibility to build a support (connection) between the structure and the frame in the place where the stiffness should be increased does not exist in many cases. An example is a quill in machine tools.

This can be solved by the new concept of mechatronic stiffness [5] as illustrated in the Fig. 1. Next to the structure 2 (performing a technological operation) another parallel auxiliary structure 3 is built. Both structures are connected by a force actuator 4. This auxiliary structure is also compliant but mainly it functions as a source of a support for force actuator 4 just like in the case of famous Archimedes quote: "Give me a place to stand, and I will move the Earth." with the only difference that this "place" does not exhibit an infinite stiffness.

The existing control mechanisms typically act in relative coordinates or are eventually brought in the structure from the outside. In this case in order to achieve collocated control in this case the position of both attaching points of the force actuator must be measured by sensors 6 with respect to the fixed reference frame 1.

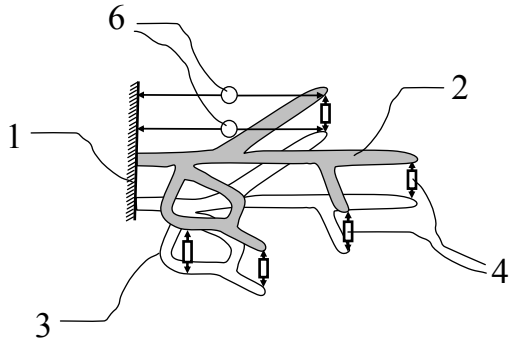

Fig. 1: Concept of mechatronic stiffness from auxiliary structure

III. SYSTEM AND CONTROL MODELING

In order to study the proposed concept of mechatronic stiffness a simple mechanic beam system has been proposed.

A. Mechatronic Two-Beam System

To illustrate the concept let us consider a single beam system as shown in Fig. 2a, where a machining tool is located at its tool center point (TCP). Disturbance force F_d acting at TCP makes the beam A to deflect. This would lead to significant errors in machining process since any deviations of the TCP directly affects machining precision.

The system (Fig. 2a) is in the next step structurally enhanced to a double beam system by a support beam B providing for additional stiffness (Fig. 2b). Piezoactuator P (with integrated displacement sensor) is placed in between beams A and B and a position sensitive sensor PSD measures the displacement of TCP. The function of the system is illustrated in Fig. 2c. Normally, the disturbance force F_d would cause the primary beam A to deflect but the feedback control system compensates for the deviation by actuating the piezoactuator P and deflecting the beam B instead of the beam A.

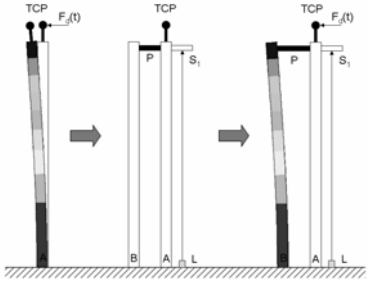

Fig. 2: Mechatronic Two-Beam System

B. Discrete Lumped Two-Mass Model

The system is modeled as a simple linear two-mass system with piezo-actuator's mass equally divided in between beams A and B as illustrated in Fig. 3. This simplification is justified since deformations allowed by the piezoactuator used are in a range of 0-60μm (effective travel range of Physik Instrumente piezoactuator PI 843.40 used in the experimental setup) and the system will operate in a range of linear elastic deformations. In Fig. 3 m_1, m_2 are the reduced masses of beams A and B, k_1, k_2, b_1, b_2 are respective stiffnesses and damping coefficients and k_s , b_s represent stiffness and damping coefficients of the piezoactuator, F_{d1} and F_{d2} represent disturbance forces.

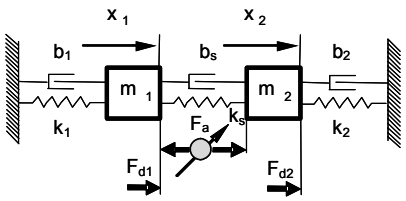

Fig. 3: Two-Mass Model

Piezoactuator model is taken from [6], [7] and it is essentially modeled as a spring with controllable free length

$$F_a = k_s(kU_{con} - \Delta\tilde{c}) \tag{1}$$

where $\Delta\tilde{c} = x_2 - x_1$, k_s represents stiffness of the piezoactuator stack, U_{con} is the piezostack control voltage (range 0-100 (V) for PI 843.40) and k is proportionality constant k = 60e-6/100 (m/V).

The controlled system can be written in matrix form.

$$\underset{\mathbf{M}}{\begin{bmatrix} m_1 & 0 \\ 0 & m_2 \end{bmatrix}}\begin{bmatrix} \ddot{x}_1 \\ \ddot{x}_2 \end{bmatrix}+\underset{\mathbf{C}}{\begin{bmatrix} b_s+b_1 & -b_s \\ -b_s & b_s+b_2 \end{bmatrix}}\begin{bmatrix} \dot{x}_1 \\ \dot{x}_2 \end{bmatrix}+\underset{\mathbf{K}}{\begin{bmatrix} k_s+k_1 & -k_s \\ -k_s & k_s+k_2 \end{bmatrix}}\begin{bmatrix} x_1 \\ x_2 \end{bmatrix}=$$
$$=\underset{\mathbf{H}}{\begin{bmatrix} -k_s k \\ k_s k \end{bmatrix}}U_{con}+\underset{\mathbf{D}_1}{\begin{bmatrix} 1 \\ 0 \end{bmatrix}}F_{d1}+\underset{\mathbf{D}_2}{\begin{bmatrix} 0 \\ 1 \end{bmatrix}}F_{d2} \tag{2}$$

Transformation into a state space description gives

$$\dot{\mathbf{x}} = \mathbf{A}\mathbf{x} + \mathbf{B}\mathrm{u} + \mathbf{E}\mathrm{z}, \quad \mathbf{x} = \left[x_1, x_2, \dot{x}_1, \dot{x}_2\right] \tag{3}$$

where

$$\mathbf{A} = \begin{bmatrix} 0 & \mathrm{I} \\ -\mathrm{M}^{-1}\mathrm{K} & -\mathrm{M}^{-1}\mathrm{C} \end{bmatrix}, \quad \mathbf{B} = \begin{bmatrix} 0 \\ \mathrm{M}^{-1}\mathrm{H} \end{bmatrix}, \quad \mathbf{E} = \begin{bmatrix} 0 \\ \mathrm{M}^{-1}\mathrm{D} \end{bmatrix}, \tag{4}$$

$$\mathrm{u} = U_{con}, \quad \mathrm{z} = \left[F_{d1} \quad F_{d2}\right]$$

C. Controllability condition

In order for the system (3) to be controllable its controllability matrix must have the rank equal to the rank of the system. The controllability matrix in the case of linear continuous systems in a the form $\dot{\mathbf{x}} = \mathbf{A}\mathbf{x} + \mathbf{B}\mathbf{u}$ is given as

$$\mathbf{R} = [\mathbf{B}, \mathbf{A}\mathbf{B}, \mathbf{A}^2\mathbf{B}, \ldots, \mathbf{A}^{n-1}\mathbf{B}] \tag{5}$$

The matrix has a specific form mainly due to a placement of the actuator in between the structural masses. From the inspection of the matrix **R** it follows that a linear combination of the first two columns can be expressed as a linear combination of the third and fourth columns if the expressions in the brackets from the first and the second row equal. Therefore, in order for the controllability matrix to have the full rank, the following condition *must not* be fulfilled (here we assume $k_s = 0$ (N/m) , $b_s = (0$ Ns/m)).

$$\left(\frac{\omega_1}{\omega_2}\right)^2 + \left(\frac{\omega_2}{\omega_1}\right)^2 + b_{r1} + b_{r2} - b_{r1}b_{r2}\left(\frac{\omega_1^2 + \omega_2^2}{\omega_1\omega_2}\right) - 2 = 0 \tag{6}$$

$$\omega_1^2 = \frac{k_1}{m_1}, \quad \omega_2^2 = \frac{k_2}{m_2}, \quad b_{r1} = \frac{b_1}{m_1\omega_1}, \quad b_{r2} = \frac{b_2}{m_2\omega_2}$$

D. Sliding mode controller

In this subsection we consider a design of a sliding mode controllers for stabilizing the state coordinate x_2 in system (3) is considered.

SMC controller has been chosen for its robustness with respect to non-parametric uncertainties, unmodelled dynamics, insensitivity to external and internal disturbances, ultimate accuracy and finite transient time [8], [9].

We follow the classical SMC design methodology extended by SMC Olgac – Elmali [8] modification where discontinuous sign function is replaced by a parameterized functional unit.

In the case of a system with two state variables suitable form of a switching manifold s parameterized by λ can be given as

$$\begin{aligned} s &= \dot{x}_2 + \lambda\, x_2 \\ \dot{s} &= f_1(\mathbf{x}, F_{d2}) + f_2(u) + \lambda\, \dot{x}_2 \end{aligned} \tag{7}$$

where

$$\begin{aligned} f_1(\mathbf{x}, F_{d2}) &= \left(\left[k_s \;\; -(k_s + k_2) \;\; b_{12} \;\; -(b_2 + b_{12})\right]\mathbf{x}^T + F_{d2}\right)/m_2 \\ f_2(u) &= k_s k u. \end{aligned} \tag{8}$$

In order for the state variables to converge to the origin parameter λ is positive and determines the sliding mode dynamics.

If we now take the control in the form

$$\begin{aligned} u &= f_2^{-1}(-f_1(\mathbf{x}, F_{d2}) - \lambda\, \dot{x}_2 - \mathrm{sgn}(s(x_2, \dot{x}_2))) = \\ &= u_{cont} + u_{disc} \end{aligned} \tag{9}$$

we obtain $\dot{s} = -\mathrm{sgn}(s)$ and the sufficient condition of sliding and approach is fulfilled for all times.

$$s\,\dot{s} \le 0 \tag{10}$$

Specifically in the case of the system (3) the control takes on the form

$$u_{cont} = -\frac{m_2}{k_s k}\left(\lambda\, \dot{x}_2 + \frac{C}{m_2}\right) \tag{11}$$

$$C = \frac{1}{m_2}\left(k_s x_1 - (k_s + k_2)x_2 + b_s \dot{x}_1 - (b_2 + b_s)\dot{x}_2\right)$$

$$u_{disc} = -\frac{m_2}{k_s k}\rho\, \mathrm{sgn}(\lambda x_2 + \dot{x}_2)$$

where $\rho > 0$ is a control gain.

In this case sliding mode constrains the dynamics of the system to a negative slope line, as can be seen in Fig. 4. Dynamics of the system is composed out of two stages. Approach stage designated in picture as 1 and a sliding stage 2 representing the discontinuous motion along the sliding manifold $s = 0$.

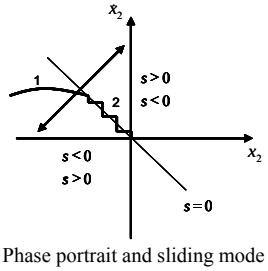

Fig. 4: Phase portrait and sliding mode domain

The adopted design is enhanced by SMC Olgac – Elmali controller synthesized in [8] using the strategy of functional unit to avoid discontinuity in control variable of the standard SMC controller. In this approach discontinuous sgn function

is replaced by a parameterized functional unit. The control u_{disc} in (9) takes on the form

$$u_{disc} = -\rho \frac{s}{|s| + \delta} = -\rho \frac{\lambda x_2 + \dot{x}_2}{|\lambda x_2 + \dot{x}_2| + \delta}. \tag{12}$$

E. LQR controller

As an alternative to the SMC the classical Linear Quadratic Regulator (LQR) controller design was also considered.
The LQR design methodology is based on an optimization approach. Given linear system

$$\dot{\mathbf{x}} = \mathbf{A}\mathbf{x} + \mathbf{B}\mathbf{u} \tag{13}$$

where $\mathbf{x}(n \times 1)$ is a state vector, $\mathbf{u}(m \times 1)$ is a vector containing control variables and **A** and **B** are corresponding system matrixes. LQR approach provides such $\mathbf{u}(t), 0 \le t \le \infty$ so as to minimize a cost functional given typically in the form of a quadratic functional

$$J = \frac{1}{2}\mathbf{x}^T(T)\mathbf{S}(T)\mathbf{x}(T) + \frac{1}{2}\int_0^T (\mathbf{x}^T\mathbf{Q}\mathbf{x} + \mathbf{u}^T\mathbf{R}\mathbf{u})dt \tag{14}$$

where $\mathbf{S}(T), \mathbf{Q}, \mathbf{R}$ are symmetrical weight matrixes, $\mathbf{S}(T), \mathbf{Q}$ are positive semi-definite matrixes and $\mathbf{R}$ is positive definite. The size of the states of interest $\mathbf{x}(t)$ is weighted by matrixes $\mathbf{S}(T), \mathbf{Q}$ relative to the amount of control action $\mathbf{u}(t)$ through the weighting matrix $\mathbf{R}$. The solution to the problem leads to the so called Riccatti differential matrix equation

$$-\dot{\mathbf{S}} = \mathbf{A}^T\mathbf{S} + \mathbf{S}\mathbf{A} - \mathbf{S}\mathbf{B}\mathbf{R}^{-1}\mathbf{B}^T\mathbf{S} + \mathbf{Q} \tag{15}$$

The equation (15) is then integrated backwards in time from $t = T$ to $t = 0$ with initial condition $\mathbf{S}_{(t=T)} = \mathbf{S}(T)$. Control action is given by time varying Kalman gain

$$\begin{aligned} \mathbf{u} &= -\mathbf{K}(t)\mathbf{x} \\ \mathbf{K}(t) &= \mathbf{R}^{-1}\mathbf{B}^T\mathbf{S}(t). \end{aligned} \tag{16}$$

It is very often a case that the Kalman gain reaches a steady state value for longer time values. If such solution $\mathbf{S}_\infty$ exists for $t \to \infty$, then it satisfies the steady state Riccati matrix algebraic equation

$$\mathbf{0} = \mathbf{A}^T\mathbf{S}_\infty + \mathbf{S}_\infty\mathbf{A} - \mathbf{S}_\infty\mathbf{B}\mathbf{R}^{-1}\mathbf{B}^T\mathbf{S}_\infty + \mathbf{Q} \tag{17}$$

and the solution to the equation (17) gives a steady state Kalman gain stabilizing the system (13).

LQR has important robustness properties [10]:

1. Upward gain margin is infinite
2. Downward gain margin is at least ½
3. Phase stability margin is at least $\pm 60^\circ$

These gain changes can occur independently and simultaneously in all m control channels.

The largest problem with LQR is the iterative design process as the provided optimal solution is in a very week relation to classical control performance specifications, such as levels of disturbance rejection, overshoot in tracking and stability margins. The fact that LQR controller is in some sense optimal does not mean that they will meet the performance goals. Since the LQR formulation does not directly allow us to achieve standard control system specifications, trial and error iteration over the values of the weights were necessary to get satisfactory controllers. More details on LQR can be found in references [11], [13].

IV. EXPERIMENTAL VERIFICATION

In order to verify the concept of mechatronic stiffness an experimental test rig was built and designed by an author.

A. Conceptual design

A conceptual scheme of the rig is shown in the Fig. 5 and Fig 6. The test rig comprises out of two steel profiles 1 and 2 with cross sections 120mm x 80mm x 4mm and the height of 450mm. The beams are firmly welded onto a steel foundation 5 and the foundation is connected to a massive cast iron plate 6 by 20mm screws 7. Moreover, beam 1 is reinforced by steal profile 3 and is also welded to the foundation 5. This adaptation was made in order to break up the system's symmetry to make the system more controllable as described in the section 3. In order to reinforce the rigidity of beam ends, reinforcement steel collars 12 have been introduced along with a stainless threaded rods 9 and 11 as shown in the top view in the Fig. 6. The rod 9 is firmly screwed to the secondary beam collar and connect directly to Physik Instrumente PI-843.40 (actuation stroke 60 μm, max. force 800 N) piezo-actuator 4. On the other side a flexible mount 8 (Fig. 6.) is used to decouple moment loads on the piezo-actuator to prevent its damage. The mount 8 is then screwed on to the threaded rod 11 and connected by nuts to the primary beam.

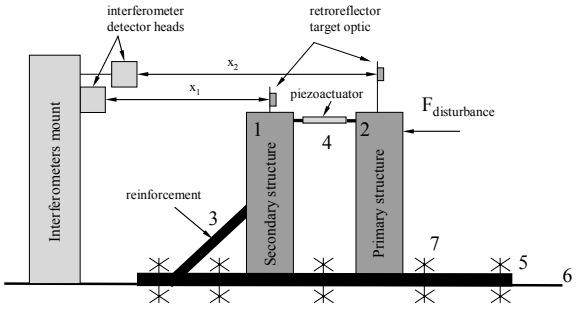

Fig. 5: Experimental concept design

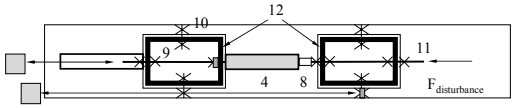

Fig. 6: Experimental concept design – top view

Displacements of beams 1 and 2 is measured by dual axis Renishaw laser interferometer RCU10 with maximum resolution of 10nm. Laser readheads are mounted onto a interferometer mount built out of aluminum construction profiles. This completes the mechanical part of the design and final realization can be seen in the Fig. 7.

Electrical part comprises out of Physik Instrumente E-662 LVPZT piezo-actuation unit and Renishaw RCU10 unit for processing the data from interferometer heads. The overall setup is controlled by an industrial PC with integrated real-time computer dSpace 1103.

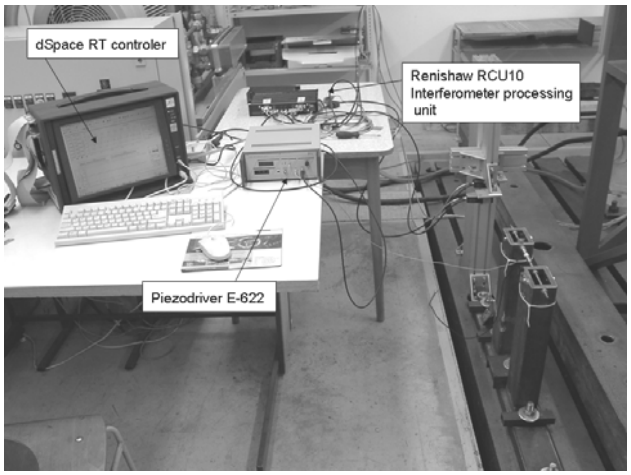

Fig. 7: Experimental setup - overview

B. Identification

The structural identification of the experimental model was carried out in order to obtain physical coefficients of the model (2). Due to the needs of the control synthesis, the physics of the experimental model was modeled as a discrete two-mass dynamics system with the parameters to be identified listed in Tab.1 below.

The first parameters to be identified were the stiffness coefficients k_1 and k_2. The next step was to identify the corresponding first eigenfrequencies so that the reduced masses could be subsequently computed. Both beams were exited by a force pulse in order to find out their modal characteristics (piezoactuator in this stage was not yet mounted). Afterwards the beams were connected by a piezoactuator and the system's impulse response to a delta pulse 0-100V with a duration of 7.52e-4s was measured.

m_1	reduced mass – beam 1
k_1	stiffness – beam 1
b_1	damping – beam 1
m_2	reduced mass – beam 2
k_2	stiffness – beam 2
b_2	damping – beam 2
k_s	piezoactuator stiffness
b_{12}	piezoactuator damping

Tab. 1: Identification parameters

In order to fit the model to the data an interactive program was written that subjected the system model to identical pulse and performed PSD of the simulated response. Systems coefficients can be changed in real time and model's PSD is being plotted against the experimental data.

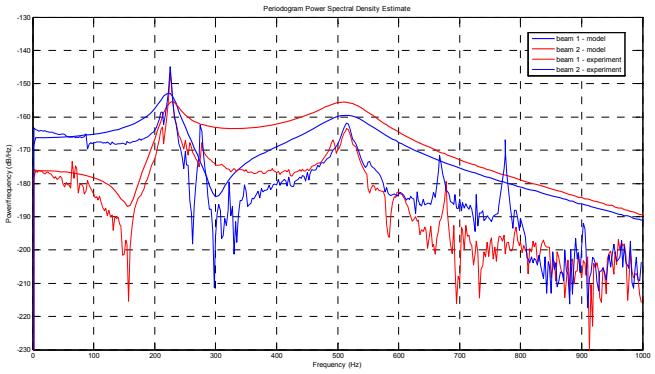

Fig. 8: System identification

Automatic tuning was not considered an option, since we wanted to have an interactive tool to see the effects of individual parameters on the systems response. In the model the previously identified values for m_1, k_1, k_2 were fixed. The values to be further tuned were therefore restricted to m_2 to account for the effects of added piezoactuator (whose mass was mainly distributed onto the s beam 2), k_s stiffness of the piezoactuator and all damping coefficients b_1, b_2, b_{12}. As it can be seen in the Fig. 8, the fit originally achieved by tuning up free parameters $m_2, k_s, b_1, b_2, b_{12}$ was quite poor and further tuning did not improve it. Structural change in the model was needed. For long time it was not clear why such a simple model cannot match the experimental data with a reasonable degree of fidelity.

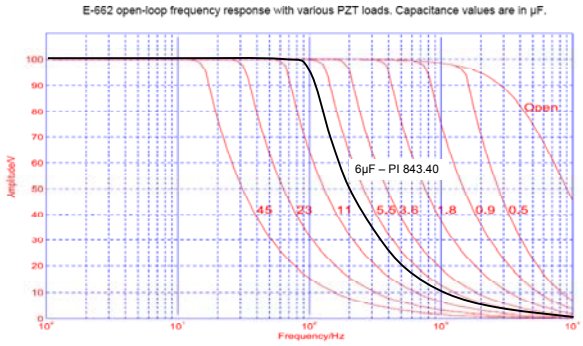

Fig. 9: E-662 Servo unit transfer function [14]

m_1	2.13 kg
k_1	7.58e6 N/m
b_1	300 Ns/m
m_2	2.44 kg
k_2	2.44e6 N/m
b_2	350 Ns/m

k_s	8.86e6 N/m
b_{12}	430 Ns/m

Tab. 2: Final identification parameters

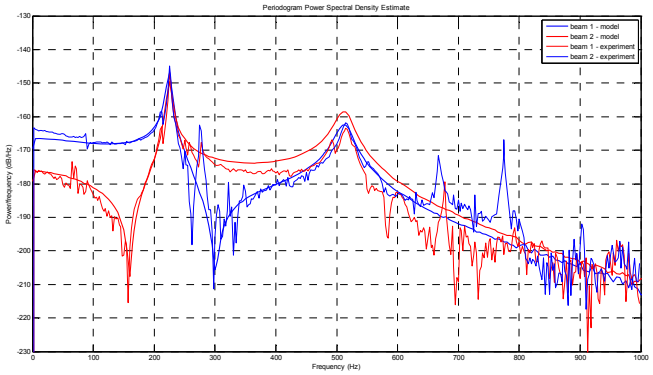

Fig. 10: System identification - final

Finally, it was identified that the problem is caused by not taking into the account E-662 piezo servodrive transfer function [14] shown in the Fig. 9.

The subsequent results along with the best fit are shown in Fig. 10. The complete identified data set for given plot is given in Tab. 2.

V. SIMULATIONS

The dynamic system (2) was coded into Simulink scheme whose core structure with two integrator chains closed by the feedback control block was used with minor modifications for all of the simulations. The used Simulink scheme is shown in the Fig. 11.

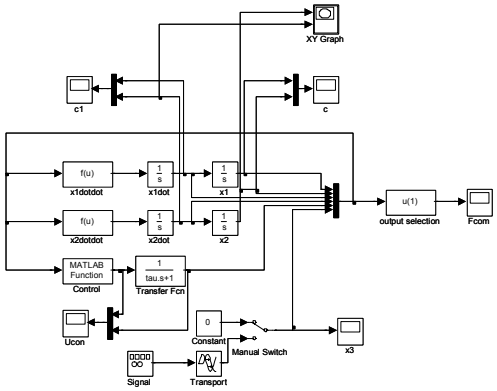

Fig.11: Simulink scheme

Generally, the primary objective of the control was to stabilize one of the beams under force disturbance treating the other as a flexible support proving for additional stiffness. Four disturbance rejection transfer functions parameterized by feedback gain **K** can be defined as

$$\frac{\mathbf{x}(s)}{\mathbf{F_d}(s)} = \begin{bmatrix} \frac{x_1(s)}{F_{d1}(s)} & \frac{x_1(s)}{F_{d2}(s)} \\ \frac{x_2(s)}{F_{d1}(s)} & \frac{x_2(s)}{F_{d2}(s)} \end{bmatrix} = \mathbf{L}\left[(s\mathbf{I} - \mathbf{A} + \mathbf{BK})^{-1} \begin{bmatrix} \mathbf{0} \\ \mathbf{M}^{-1}\mathbf{D}_1 \end{bmatrix} \quad (s\mathbf{I} - \mathbf{A} + \mathbf{BK})^{-1} \begin{bmatrix} \mathbf{0} \\ \mathbf{M}^{-1}\mathbf{D}_2 \end{bmatrix} \right] \quad (18)$$

where $\mathbf{L} = \begin{bmatrix} 1 & 0 & 0 & 0 \\ 0 & 1 & 0 & 0 \end{bmatrix}$ is a corresponding selection matrix, $\mathbf{A,B}$ are system matrixes from (3) and $\mathbf{M},\mathbf{D}_1,\mathbf{D}_2$ matrixes from (2), matrix $\mathbf{K}$ contains feedback gains. From the application point of view only the matrix components of dynamic compliance $G_{11}(s) = \frac{x_1(s)}{F_{d1}(s)}$ and $G_{22}(s) = \frac{x_2(s)}{F_{d2}(s)}$ are of an interest. Absolute values of dynamic compliance of an uncontrolled system $G_{11}(s)$ and $G_{22}(s)$ are plotted in the Fig. 12 illustrating also an effect of increasing the cross-coupling stiffness k_s.

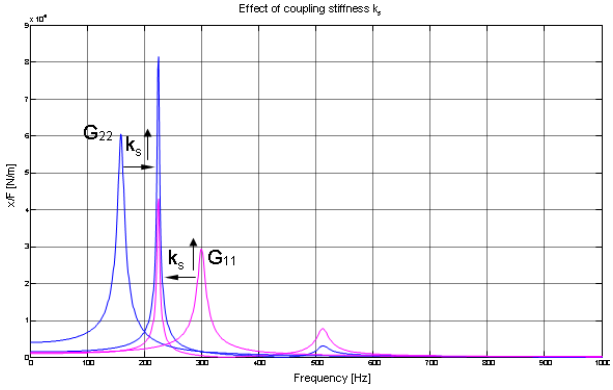

Fig. 12: Dynamic compliance $G_{11}(s)$ and $G_{22}(s)$

According to LQR design methodology symmetric weight matrixes $\mathbf{Q},\mathbf{R}$ for the controlled system (2) were chosen in order to decrease the dynamic compliance (the inverse of dynamic stiffness) of beam 1 or beam 2 according to system performance index respectively as follows:

A. increase of dynamic stiffness - beam 1 - LQR

$$\mathbf{R} = [1], \quad \mathbf{Q} = \begin{bmatrix} 5e15 & 0 & 0 & 0 \\ 0 & 1 & 0 & 0 \\ 0 & 0 & 5e13 & 0 \\ 0 & 0 & 0 & 1 \end{bmatrix} \quad (19)$$

This selection gives a major penalty on displacement of beam 1 and also contains high penalty on its velocity. The control matrix **R** was chosen as 1 so as to give no restrictions on control effort. Resulting control feedback gain matrix has values, $\mathbf{K}_{\text{beam1}}$= 1e7 *[-6.8174 -0.1690 -0.7071 -0.0000] and places system eigenvalues at the locations s = [-1.76e7, -9.22e0+1.00e3i, -9.22e0-1.00e3i, -1.00e1]. The control changes completely the dynamics of the original uncontrolled system.

The Fig. 13 illustrates how the corresponding feedback affects the system dynamics in frequency domain. Resulting graphs have been obtained from analytical expressions given in (18). It can be observed that dynamic compliance of the

stabilized beam 1 significantly decreased, especially in higher frequency range and that the only small resonance peak occurs at the supporting beam's natural frequency 160Hz.

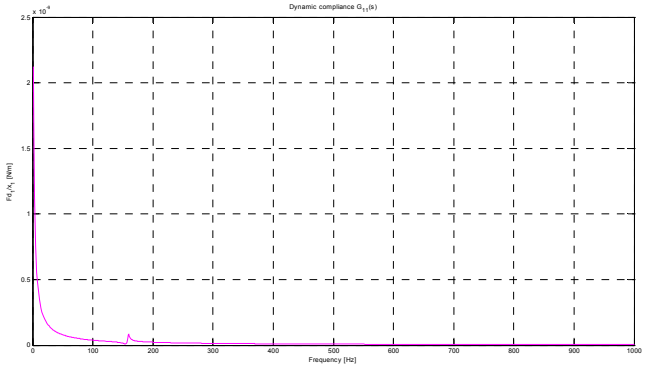

Fig. 13: Decrease of dynamic compliance of beam 1 by active control

B. increase of dynamic stiffness - beam 2 - LQR

$$\mathbf{R} = [1] \ , \quad \mathbf{Q} = \begin{bmatrix} 1 & 0 & 0 & 0 \\ 0 & 5e15 & 0 & 0 \\ 0 & 0 & 1 & 0 \\ 0 & 0 & 0 & 5e13 \end{bmatrix} \tag{20}$$

For the purpose of comparison the gains in the matrix $\mathbf{Q}$ and $\mathbf{R}$ were chosen identical to the ones it the previous case. Resulting control feedback gain matrix has values,

$\mathbf{K}_{\text{beam2}}$ = 1e7* [0.1661 6.8633 0.0000 0.7071] and places system eigenvalues at the locations s =[-1.54e7, -1.41e1 +1.89e3 i, -1.41e1-1.89e3i, -1.00e1].

The opposite signs of respective control gains in $\mathbf{K}_{\text{beam1}}$ and $\mathbf{K}_{\text{beam2}}$ reflect the fact that the system is separated by action and reaction force: positive force exerted on beam 1 equals negative force acting on beam 2 and vice versa.
Fig. 14 shows how the corresponding feedback affects the system dynamics in frequency domain. Resulting graphs have been obtained from analytical expressions given in (17) . It can be observed that dynamic stiffness of the stabilized beam 2 significantly increased, especially in higher frequency range and only very negligible resonance peak occurs as the resonance frequency of the supporting beam 1 at around 300Hz.

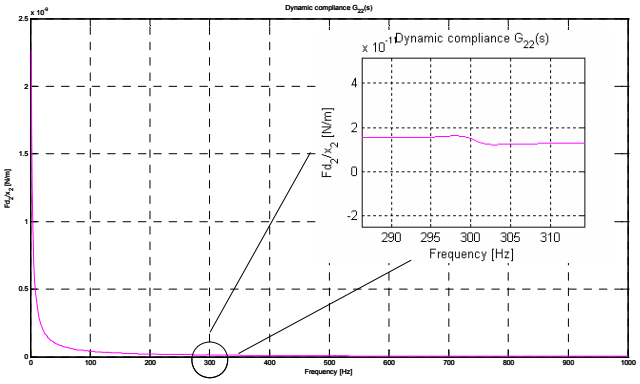

Fig.14: Decrease of dynamic compliance of beam 2 by active control

SMC controller has been implemented according to Olgac-Elmali design methodology described in the control section 3. The initial conditions and disturbance force acting on the beams were the same as in the case of LQR controller in previous section. Controller's specific parameters were chosen as: $\lambda = 100$, $\rho = 50$ and in the case of increasing dynamic stiffness of the beam 2 the parameter d was varied between d =1e-7 a d =1e-3 in order to show its effect on controllers performance.

C. increase of dynamic stiffness - beam 1 - SMC

The performance of the controller in time domain is shown in the Fig. 15, where disturbance force with aplitude 40N and frequency 300Hz starts to act on beam 1 at 0.1 s.

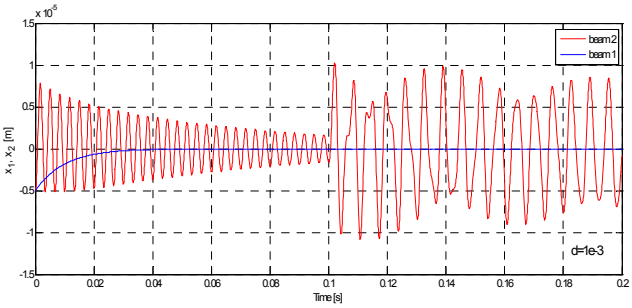

Fig. 15: Disturbance rejection – time domain

D. increase of dynamic stiffness - beam 2 - SMC

The performance of the controller in time domain in the case of increasing the dynamic stiffness of the beam 2 is shown in the Fig. 16, along with the required control action for two different values of parameter d .

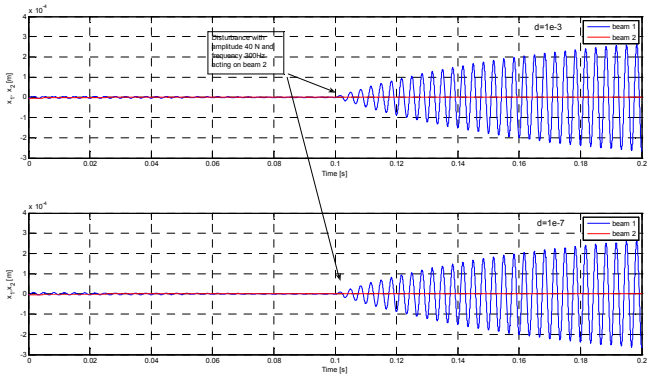

Fig.16: Disturbance rejection – time domain

The Fig. 17 shows the sliding action in $x - \dot{x}$ domain and its disruption under disturbance force in the case of $d = 1e-3$ when control action is not able to effectively compensate for the disturbance.

From the simulation results it can be concluded that both regulators can be used to control the structural model. Generally SMC controller is easier to tune as it has fewer

tunable parameters and these parameters relate more intuitively to the dynamics of system.

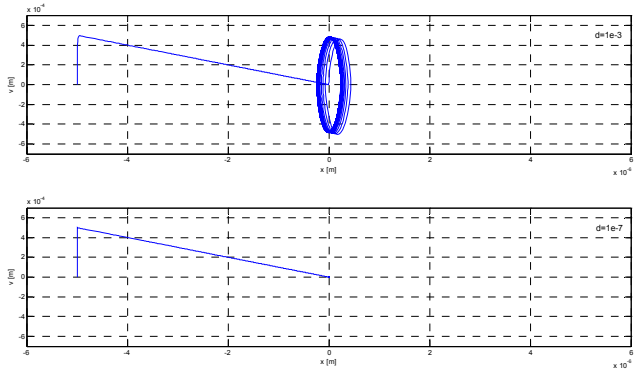

Fig.17: Disturbance rejection – limit cycling

VI. EXPERIMENTAL RESULTS

The goal of the experimental stage was to verify the findings from the previous section and to test the ranges of its validity in the reality. This has proven to be the most difficult part. Obtaining conclusive results has proven to be extremely difficult. Only LQR control is currently implemented.

One of the most serious fundamental limitations is related to the quality of feedback signals. The second fundamental limitation is the piezoactuators performance given by gain transfer function in the Fig. 9. The data sheet unfortunately does not provide any information concerning the phase lag response. The complete transfer function of the piezoactuator is to be measured in the future research.

The third fundamental limitation as discussed in section 3 is the system's loss of controllability under special conditions given by (6) causing the system to be extremely sensitive to noise sources amplified in the feedback loops. The situation is severe not only when the condition is precisely met but also in some of its vicinity. With the highly quantized feedback signals this is a serious problem.

The fourth fundamental problem was the non-collocation of sensors and actuators. Originally the lasers mount was mounted just directly next to the double beam system so as to filter out disturbances entering the system from the outside (massive traffic). At the end it proved to be necessary to expose the lasers mount to noise sources in the exchange of breaking up the energy transfer between the double beam system and laser mount causing the system to be unstable even under very small gains.

During the transportation of the system from iron plate to the concrete base foundation unfortunately the original piezoactuator P-843.40 was destroyed and a drop in replacement had to be used in order to finish the experimental part. This piezoactuator P-845.40 has equal stroke but is 100 g heavier and produces push/pull forces in range 3000/700 N. It has electrical capacitance 24μF and 3 times higher stiffness. Due to time limitations, it was impossible to perform new identification and modeling. Bringing model and experiment to a good fit will be a subject of the future research.

A. Increasing dynamic stiffness of the beam 1

Application was created in ControlDesk (interface software between PC and the dSpace 1103 computer) that enables to control, tune and log all of the relevant experimental signals. Feedback gains were adjusted manually under a guidance of results from LQR investigations up to the maximum values until instability occurred. The maximum achievable gains were $\mathbf{K}_{exp\_beam1}$ = 1e7 *[-4.5000 -0.1700 -0.0005 -0.0000].

As it can be seen from the comparison with the gain matrix in section 5, all values except for the velocity gain fit well with the gains modeled by LQR. Due to quantization problems velocity gain had to be kept very low in order not to introduce too much of a noise amplification into the control loop. The response of the system on the excitation of the beam 1 by a modal hammer is shown in the Fig. 18. The first graph depicts the displacement of the beam 1, the second graph depicts the displacement of the beam 2, the third graph corresponds to the force as captured by dSpace from the modal hammer. The very bottom graph shows the control signal entering the E-662 piezo servo unit. In order to gain a better insight power spectra denisity (PSD) of the control pulse from the Fig. 18 along with PSD of uncontrolled system and time responses of the beam 2 in controlled and uncontrolled case were computed. Modul of the frequency transfer function (in our specific case - dynamic compliance) can be computed from PSD values.

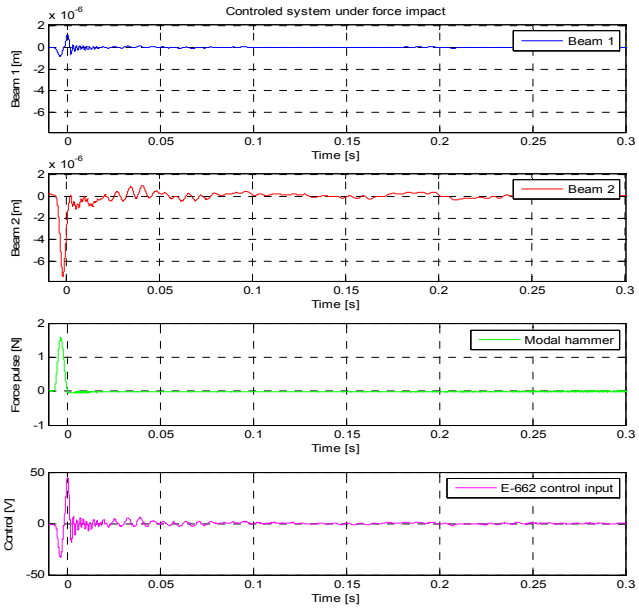

Fig. 18: Controlled System: Beam 1 – force impact

Absolute value of the module of the transfer function $H(f)$ is equal to a square root of $S_y(f)/S_x(f)$. Relative increase of the dynamic stiffness of the controlled beam 1 with respect to uncontrolled system is plotted for comparison purposes in the Fig. 19. This graph represents the most significant

experimental result as it shows in detail how the control affects the ability of beam 1 to resist disturbance forces at various frequencies.

It can be concluded, that the control effectively increases the dynamic stiffness in all frequency ranges up to around 260Hz, where the increase in frequency range up to 50Hz is the most predominant. Also, it is can be seen that the first eigenfrequency of the original system is effectively suppressed (virtually eliminated!).

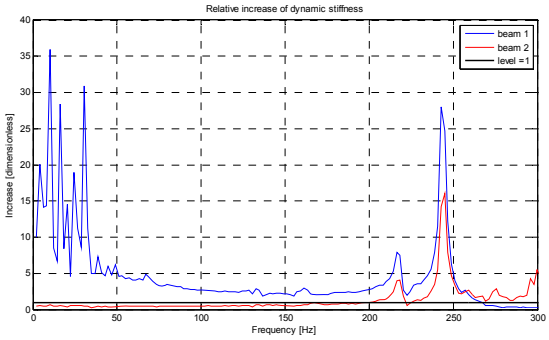

Fig. 19: Dynamic stiffness relative increase - controlled versus uncontrolled system

B. Increasing dynamic stiffness of the beam 2

Similar results for the increasing the dynamic stiffness of the beam 2 were expected, however, the problem of stabilizing the more compliant beam 2 remains an unsolved problem as it was not possible to achieve system stability for *any* combination of gains predicted by LQR. The system is *extremely* sensitive to positive gain closed around the beam 2, and the velocity signal from beam 2 is not able to stabilize the system for any feasible value and makes the system go into resonance around the systems 1st eigenfrequency at 225Hz. As mentioned, the problem may be related to signal quantization problems and/or a spillover effect of unmodelled modes destabilizing the system. This problem presents one of the most challenging future research topics.

For the reasons above the experimental results are still considered primarily as a guidance and the gained experience is going to be used to build a second generation test rig.

VII. Conclusion

Stabilization of the stiffer beam was obtained with relative ease, however, the more compliant beam 2 it proved to be impossible to stabilize and even very small gains set the whole system into resonance around its first structural mode. This problem requires further investigations.

The experimental part proved to be the most challenging. However, it can be concluded that the concept of mechatronic stiffness is feasible and it is the most important feature: the ability to successfully suppress the limitation of the first eigenfrequency of the primary structure can be realized. To prove this more conclusively in reality a new modified test rig is to be built.

From the practical point of view the proposed technology lends itself to a possible use in a variety of industrial setups ranging from vibration control of high precision coordinate measuring machines, active vibroisolation of sensitive devices all the way down to the machine tools industry [15].

As a viable practical machine tools application a mechatronical quill is proposed. This device should be able to actively compensate for the gravity, flexibility and temperature induced errors that often arise in deep boring applications. The proposed device is illustrated in the Fig. 20 and consists of two co-centric tubes with piezoactuators placed in between. The collocated control is enabled through laser measured tip deviations as illustrated.

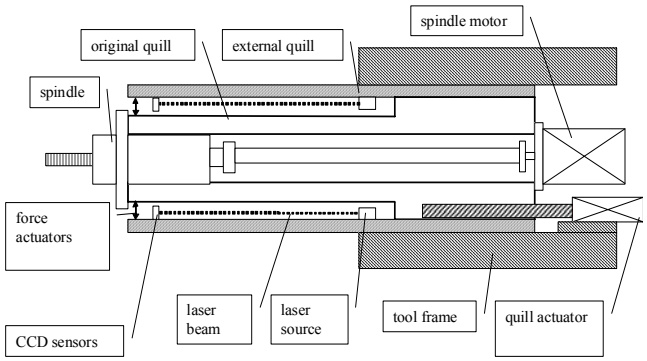

Fig. 20: Mechatronical quill

Another area where the developed technology could find its use is active vibration control of attachments of high-speed milling spindles. The parasitic oscillations leave their signature on the work piece. The proposed technology of mechatronic stiffness might improve the overall surface quality and increase the compliance induced errors.

Apart from vibroisolation and mechatronical stiffness, it should be mentioned, that the proposed device can be also operated in a micro-manipulator mode and not only in stabilization mode. This would make it a viable device in areas where micromanipulation is in use e.g. semiconductor industry, biotech or high precision manipulations where positioning in nanometer ranges is required.

Acknowledgment

The authors appreciate the support by the project “Increase of structural stiffness by means of mechatronic principles” GACR 101/08/P633.

References

[1] Ehmann, Ch., Nordmann, R.: Low Cost Actuator for Active Damping of Large Machines Mechatronics 2002 Conference, California, Berkeley Dec. 2002.

[2] http://www.piezomechanik.com – Piezomechanical Stack actuators, Information materials

[3] Enver E. et al. Pro-Active Chatter Reduction, www.mmsonline.com/articles/069803. html.

[4] Lee, A.G., Suh, J. G. et al.: Design and Manufacture of Composite High Speed Machine Tool Structures. In Composites Science and Technology. Issue 64, pp. 1523–1530, 2004.

[5] Valášek, M.: Method and Device for Change of Stiffness of Mechanical Constructions, PV2006-123, Patent application (in Czech).

[6] Šika Z.: Active and Semi-active Vibration Suppression of Machines, Habilitation Thesis, Czech Technical University in Prague, Prague, 2004 (in Czech).

[7] Kejval, J.: Semi-active Vibration Suppression of Machines by Semi-active Vibration Absorber, PhD. Thesis, Czech Technical University in Prague, Prague, 2001 (in Czech).

[8] Levant, A: Higher Order Sliding Modes, Differentiation and Output-Feedback, Int. Journal of Control,, Vol. 76, Nos 9/10, pp. 924-941, 2003.

[9] Olgac N., Elmali H.: Robust Control of Articulated Arms via Variable Structure Control Method. In 8st World. Congress on the Theory of Machines and Mechanisms,, pages 643–646, Prague, August 26-31, 1991.

[10] Levine, W., S., et al.: CRC Control Handbook , CRC Press, 1995.

[11] Valášek, M., et al.: Mechatronics, Publishing House of ČVUT, Praha, 1995 (in Czech).

[12] Instruction manual – Melservo – MR-J2S-A Servo Amplifier, Mitsubishi Electric – Industrial Automation, 2004.

[13] Havlena, V., Štěcha, J.: Modern control theory, Publishing House of ČVUT, Praha, 1996 (in Czech).

[14] Physik Instrumente GmbH.: Piezo servo E-622 Data Sheet.

[15] Valášek, M. et al.: Mechatronical quill, Project proposal MPO, ČVUT FS, Praha, 2004 (in Czech).